Insights into the radical-radical and radical-substrate dimerization processes for substituted phenylmethylenepyrans

Laurianne Wojcik, Isidoro López, Sebastien Gauthier, Nolwenn Cabon, Pascal Le Poul, Frederic Gloaguen, Nicolas Le Poul

Insights into the radical-radical and radical-substrate dimerization processes for substituted phenylmethylenepyrans

Laurianne Wojcik,[a] Isidoro Lopez,[a] Sébastien Gauthier,[b] Nolwenn Cabon,[b] Pascal Le Poul,[b] Frédéric Gloaguen,[a,*] Nicolas Le Poul[a,*]

[a] *Laboratoire de Chimie, Electrochimie Moléculaire et Chimie Analytique (CNRS UMR 6521), Université de Bretagne Occidentale, 6 Avenue Le Gorgeu, CS 93837, 29238 Brest, France*

[b] *IUT de Lannion, CNRS UMR 6226, Institut des Sciences Chimiques de Rennes, Université de Rennes 1, Rue Edouard Branly, 22300 Lannion, France*

*Corresponding authors : nicolas.lepoul@univ-brest.fr; frederic.gloaguen@univ-brest.fr

Abstract

The electrochemically-induced C-C bond making/breaking for six differently R-substituted phenylmethylenepyrans has been investigated by voltammetry in organic media. All compounds display an irreversible oxidation peak whose potential is fully dependent on the electrophilic property of the substituent R. The electrochemical oxidation yields bis-pyrylium compounds by σ-σ C-C bond formation. The initial methylenepyrans are recovered by cleavage of the C-C bond through electrochemical reduction of the bis-pyrylium species. According to the voltammetric analysis, the mechanistic pathway, radical-radical or radical-substrate, for the intermolecular dimerization is fully R-dependent. Electronic structure

calculations show that the spin population in the radical cation and the strength of the σ-σ C-C bond in the dimer strongly depend on the nature of R. In addition, low-temperature electrochemical voltammetry (175 K), and room-temperature high scan rate cyclic voltammetry have been used to unravel the kinetics of the C-C bond formation.

Keywords : radical dimerization ; methylenepyran ; low-temperature voltammetry ; C-C bond making ; ab initio calculations.

1. Introduction

The reversible dimerization of organic radicals has for a long time fascinated electrochemists, essentially because the analysis of the experimental data, in particular cyclic voltammetry (CV) and chronoamperometry (CA), can give straightforward information on the mechanism of dimerization as well as the kinetics/thermodynamics of the process [1-8]. Different types of organic dimers can be found according to the mode of interaction between monomeric units, upon redox activation. Most of studies have been focused on organic dimers generated by the formation of σ-σ carbon-carbon bond [9-11]. Also, π-π dimers have been more recently developed with supramolecular organic systems [12-15]. While most of reported studies have been carried out for fundamental purposes, recent works have shown some remarkable applications in the domain of redox switches and electrochromic devices for systems displaying optical properties in the UV-Visible spectroscopic domain [9, 11, 16-20]. Among them, methylenepyrans (MPs) are organic molecules which have been fully exploited as dyes for photovoltaic cells [21], but also as component parts of push-pull compounds for non-linear optic (NLO) applications and luminescent devices [22-24]. As their dithiafulvalene (DTF)

analogues [25], MPs are able to form σ–σ C-C bound dimers upon oxidation at a relatively low redox potential. The generated bis-pyrylium compounds can be reduced chemically and electrochemically to yield back the initial MPs. Our experimental and computational studies on a series of substituted-MPs have emphasized that the redox and spectroscopic properties of these compounds could be modulated by adequate variation of the substituting group [26-30]. Noteworthy, we recently demonstrated by time-resolved spectroelectrochemistry that R-substituted phenyl-MPs **1a-f** (Scheme 1) could be switched between their mono-pyran and bis-pyrylium states by redox triggering over several cycles, leading to a concomitant change of their spectroscopic signatures [26]. Moreover, the electrophilic character of the substituting group R on the phenylmethylene moiety (Scheme 1) was shown to affect in a significant manner the oxidation potential of the MP. Contrarily, the reduction potential of the bis-pyrylium species **(2a-f)**$^{2+}$ remained almost insensitive to the nature of the R group. These experimental results were fully supported by electronic structure and thermochemical calculations [26]. In complement to these first results, we present here our further investigations on the dimerization mechanism and the kinetics associated to the oxidation of compounds **1a-f**, by the combination of electrochemical and computational approaches. In particular, the influence of the R-substituting group on the dimerization process has been deeply explored, with the help of low-temperature and high scan rate cyclic voltammetry.

Scheme 1

Scheme 1. C-C bond making/breaking by oxidation of R-substituted phenylmethylenepyrans **1a-f** and reduction of their bis-pyrylium derivatives **(2a-f)**$^{2+}$.

2. Experimental section

2.1 Synthesis of compounds 1a-f

All syntheses and characterization of the phenylmethylenepyran derivatives **1a-f** were previously reported [26].

2.2 Electrochemical methods

The electrochemical studies were performed in a glovebox (Jacomex) (O_2 <1 ppm, H_2O <1 ppm) with a homemade three-electrode cell (WE, Pt; RE, Ag wire; CE, Pt), such that the volume of the solution (hence concentration) was constant all over the duration of measurement (no need for gas bubbling). Ferrocene was added at the end of each experiment to determine the redox potential values. The potential of the cell was controlled by an AUTOLAB PGSTAT 100 (Metrohm) potentiostat monitored by NOVA software (Metrohm). Dichloromethane was freshly distilled from CaH_2 and kept under argon in the glovebox. The supporting salt NBu_4PF_6 was synthesized from NBu_4OH (Acros) and HPF_6 (Aldrich). It was then purified, dried under vacuum for 48 h at 100 °C, and kept under N_2 in the glovebox.

Low-temperature voltammetric measurements were performed with a specific home-designed schlenk-type cell (WE: Pt, RE: Pt wire, CE: Pt wire). The cell was introduced at room temperature under nitrogen in a liquid nitrogen cryostat (LN2 Oxford Instruments) [31]. Temperature was adjusted with a temperature controller (ITC Mercury) connected to the cryostat. The temperature inside the electrochemical cell was also checked by a supplementary thermocouple (Pt1000, VWR, resolution 0.1 K).

2.3 Theoretical methods

Calculations were carried using the so-called Hartree-Fock-3c (HF-3c) method as implemented in the Orca 3.03 software [32, 33]. The HF-3c method includes correction terms for London dispersion interactions, basis set superposition error, and basis set deficiency effects. Geometry optimizations and single-point calculations were carried out with a tolerance of 10^{-8} hartree on energy change. Electronic structures of singly charged species (i.e. open shell) were calculated using the unrestricted HF method. The preparation of the input files and analysis of the output files was carried out using the Avogadro 1.03 software [34]. The input structures for the geometry optimization in the gas phase of **1a**, $\mathbf{1a}^{+\bullet}$, **1f** , $\mathbf{1f}^{+\bullet}$, as well as $\mathbf{2}^{+}$ and $\mathbf{2}^{2+}$ dimers (for R = NMe_2, H or NO_2) were manually built from the X-ray structures of **1b** and $[BisFcMP]^{2+}$, respectively [26, 30]. A vibrational frequency calculation was carried out on each of the structures to confirm that the stationary point is a minimum in energy and to obtain the free energy correction term. Effect of the solvent (i.e. CH_2Cl_2) was accounted for using a conductor-like screening model (COSMO) as implemented in the Orca 3.03 software [35].

3. Results and Discussion

3.1 Electrochemical studies

Cyclic voltammetric (CV) studies of compounds **1a-f** have been first carried out at a Pt working electrode in dichloromethane at room temperature. As previously stated [26], all PhMPs display the same redox behavior, i.e. a single irreversible oxidation peak on the forward scan at $E_{pa}(1)$ and an irreversible reduction peak on the backward scan at $E_{pc}(2)$ (see Table 1 for electrochemical data), the value of $E_{pa}(1)$ and $E_{pc}(2)$ varying with R. For example, Fig. 1 displays the CV obtained for **1a** at v = 0.1 $V.s^{-1}$ and C = 1 mM. The same current density was obtained for all methylenepyran compounds [26]. Scanning initially in negative direction, by CV or Rotating Disk Electrode Voltammetry (RDEV), does not show any cathodic process except for the nitro derivative, as previously reported [26] (see Fig. S3 for

CV and RDEV). Exhaustive electrolyses at $E_{pa}(1)$ lead to the formation of the bispyrylium derivatives **(2a-f)$^{2+}$**[26]. Coulometric measurements indicate that that the process is monoelectronic (i.e. two electrons for the oxidation of two molecules of phenylmethylenepyrans). For all R-substituted compounds, the resulting species are irreversibly reduced at $E_{pc}(2)$, in agreement with CV studies.

Fig. 1

Fig. 1. CV (v = 0.1 V.s^{-1}) at a Pt electrode (diam. 3mm) of compound **1a** (C = 1mM) in CH_2Cl_2/NBu_4PF_6 0.1 M under argon at T = 293 K.

Table 1. Electrochemical data for compounds **1a-f** and **(2a-f)$^{2+}$** in CH_2Cl_2/NBu_4PF_6 0.1 M.

	R	$E_{pa}(1)$[a]	$E_{pc}(2)$[a]	$dE_{pa}(1)$ / $d\log v$[b]	$dE_{pa}(1)/d\log C$[c]	**Dimerization mechanism**[d]
1a	H	0.22	-0.85	33.3	-30.2	RSD
1b	NMe_2	-0.17	-0.83	21.3	-17.2	RRD
1c	OMe	0.14	-0.81	22.9	-20.6	RRD
1d	CO_2Me	0.34	-0.77	34.1	-37.9	RSD
1e	Br	0.29	-0.78	32.7	-31.4	RSD
1f	NO_2	0.41	-0.73	32.1	-38.0	RSD

[a] Data obtained at v = 0.1 V.s^{-1} and C = 0.5 mM with ohmic drop correction; [b] Determined from data obtained at C = 0.5 mM for 0.02 V.s^{-1} < v < 1 V/s with ohmic drop correction; [c] Determined from data obtained at v = 0.1 V.s^{-1} with ohmic drop correction for 0.05 < C < 0.5 mM. [d] Abbreviations for : RSD: Radical-Substrate Dimerization; RRD: Radical-Radical Dimerization.

As previously stated [26], monoelectronic oxidation at $E_{pa}(1)$ leads to the dimerization of the phenylmethylenepyran. The generated bis-pyrylium is further reduced at $E_{pc}(2)$, inducing the cleavage of the generated C-C bond, and yielding back the initial species. The value of $E_{pa}(1)$ is strongly dependent on the electrophilic nature of the R substituting group (ΔE_{pa} (1) = 580 mV). Such a result was previously ascribed to the location of the electronic density on both the substituted phenyl and pyran rings for **1a-f**. In contrast, the peak potential value at $E_{pc}(2)$ is less affected by the substituent R (ΔE_{pc} (2) = 120 mV), the highest value being obtained for the nitro compound. This suggests that the electron transfer reaction merely occurs on the pyrilium moiety and not on the substituted phenyl groups, in full agreement with previous theoretical studies [26].

Fig. 2

Fig. 2. Plots of E_{pa} *vs*. log *v* for compounds A) **1a** (R=H); B) **1b** (R=NMe_2); C) **1c** (R=OMe); D) **1d** (R=CO_2Me); E) **1e** (R=Br); F) **1f** (R = NO_2); (*C* = 0.5 mM).

In order to further investigate the C–C bond making/breaking mechanism, variation of the anodic peak potential $E_{pa}(1)$ with voltammetric scan rate and concentration has been measured for **1a-f**. Fig. 2 displays plots of $E_{pa}(1)$ against log *v* for *C* = 0.5 mM obtained for the six organic dyes. Clearly, the variation is linear in agreement with the occurrence of coupled chemical and electrochemical reactions. Interestingly, full analysis of the experimental data in the 0.05 to 1.00 mM concentration range shows that the slope value from ($E_{pa}(1)$ *vs*. log *v*) plots remains constant up to 0.5 mM (Fig. 3).

Fig. 3

Fig. 3. Plots of slope of (E_{pa} *vs*. log *v*) against log *C* for **1a-f**.

The values of the slope at a concentration of 0.5 mM for all studied phenylmethylenepyrans **1a-f** are given in Table 1. Two different behaviors are clearly observed. When R = NO_2, CO_2Me, Br and H, a slope of *ca.* 30 mV/decade is obtained. With better donor groups such as R = NMe_2 and OMe, the slope is rather close to 20 mV /decade. The effect of the R group can also be observed when analyzing the variation of the anodic peak $E_{pa}(1)$ with the concentration in compound **1a-f** at a moderate scan rate (v = 0.1 $V.s^{-1}$). Plots of $E_{pa}(1)$ *vs*. log *C* are linear, as shown in Fig. 4 for all compounds. However, the analysis gives two different slope values according to the nature of R. Hence, it is close to -20 mV/decade for derivatives bearing electrodonating groups (NMe_2, OMe), while the four other compounds display a -30 mV/decade value (Table 1). Noteworthy, according to the classical treatment of dimerization process, these data indicate that the R moiety has a strong influence on the mechanism of dimerization. With withdrawing groups such as NO_2, dimerization occurs merely through a radical-substrate process (RSD) whereas radical-radical reaction (RRD) is preferred as the donor effect of the R group increases as depicted in Scheme 2.

Fig. 4

Fig. 4. Plots of E_{pa} vs log *C* for compounds A) **1a** (R=H); B) **1b** (R=NMe_2); C) **1c** (R=OMe); D) **1d** (R=CO_2Me); E) **1e** (R=Br); F) **1f** (R = NO_2); (v = 0.1 $V.s^{-1}$).

Scheme 2.

Scheme 2. Schematic pathway for the C-C bond making/breaking of R-substituted phenylmethylenepyran **1a-f** compounds upon electron transfer. Inset: RRD *vs*. RSD mechanisms.

Further investigation of the dimerization process was then carried out by low temperature electrochemistry, in order to find better conditions to obtain a reversible system by CV for the monoelectronic oxidation of the phenyl-MP into its pyrylium cation. As shown above, variation of the scan rate between 0.02 $V.s^{-1}$ and 5 $V.s^{-1}$, or decrease of the concentration in phenyl-MP (0.04 mM < *C* < 1 mM) did not induce any appearance of reversibility within the defined ranges, meaning that the dimerization process is fast *vs*. timescale of the CV measurements. We then took advantage of a cryo-electrochemical setup [31, 36], developed by some of us to slow down the kinetics of the chemical process, for the eventual detection of the reduction peak of the electrochemically-generated radical cation $\mathbf{(1a\text{-}f)^{+\bullet}}$ at $E_{pc}(1)$. The cryo-set-up consists in a home-designed air-tight electrochemical cell which can be introduced in a liquid nitrogen cryostat, hence allowing electrochemical measurements above the freezing point of the liquid electrolyte.

Fig. 5

Fig. 5. CVs (v = 0.1 $V.s^{-1}$) at a Pt electrode (diam. 1mm) of compound **1d** (0.04 mM) in CH_2Cl_2/NBu_4PF_6 0.1 M under argon for 175 K < *T* < 183 K.

Fig. 5 displays the voltammetric response at very low temperatures (175 K < T < 183 K) in CH_2Cl_2/NBu_4PF_6 of **1d** in a relatively low concentration (C = 0.04 mM) and moderate scan rate (v = 0.1 V.s^{-1}). CV shows that the decrease of the temperature induces a significant increase of the $E_{pa}(1)$-$E_{pc}(2)$ peak-to-peak separation. For instance, this value reaches 1.36 V at T=183 K whereas it is equal to 1.11 V at room-temperature. Such effect can be ascribed to a decrease of the electron transfer kinetics for each process (**1**$^{+\bullet}$/**1** and **2**$^{2+}$/**2**) with T. More importantly, the anodic peak at $E_{pa}(1)$ remains chemically irreversible, even at 175 K or by increasing the scan rate (up to 1 V.s^{-1}), showing that even under these conditions, the dimerization process remains fast (*vs.* timescale of the experiment).

We then opted for another approach consisting in increasing substantially the scan rate at room temperature in diluted solutions, such that the kinetics of the C-C bond formation could be attained. An example is given with the dimethylamino derivative **1b** for which high scan rate CV at v = 100 V.s^{-1} induces the appearance of a cathodic peak corresponding to the reduction of the electrochemically generated radical cation **1b**$^{+\bullet}$ at $E_{pc}(1)$ with concomitant decrease of the reduction peak of the bispyrylium **2b**$^{2+}$ (Fig. 6, black curve). However, no oxidation peak of the transient bis-pyran species **2b** was detected, even at this scan rate, in agreement with a very fast dissociative C-C bond breaking process.

Fig. 6

Fig. 6. Experimental (black) and simulated (red) CVs at A) v = 100 V.s^{-1} and B) v = 1 V.s^{-1} of compound **1b** (C = 0.09 mM) at a Pt electrode (diam. 1mm) in CH_2Cl_2/NBu_4PF_6 0.1 M. (for details, see Appendix A).

Voltammetric analysis of the **1b**$^{+\bullet}$**/1b** redox system at this scan rate allows the determination of the standard potential (E^0(1) = -0.12 V vs Fc). Moreover, according CV analysis (see above), **1b** dimerizes through a radical-radical coupling upon oxidation. Hence, the dimerization rate constant, k_{dim}, can determined by using the equation (1) [37] :

$$E_p = E^0 = 0.903\frac{RT}{F} - \frac{RT}{3F}\ln\left(\frac{4RTk_{dim}C}{3Fv}\right) \qquad (1)$$

The k_{dim} term can be extracted from the intercept value from plots of E_{pa} *vs.* ln *v*. Our calculations give an average value for k_{dim} = 4.2 (+/-0.7) 10^7 $M^{-1}.s^{-1}$ averaged from three different concentrations in compound **1b** (*C* = 0.40 mM, 0.19 and 0.09 mM). The calculated k_{dim} value found illustrates a fast dimerization process, in good agreement with previous studies on a dithiafulvene analogue which also performs a radical-radical dimerization upon oxidation (k_{dim} =2 10^8 M^{-1} s^{-1}) [25]. Alternatively, voltammetric simulation has been carried out by using the DigiElch© software by assuming an EC_{dim} mechanism and k_{dim} = 9 10^6 $M^{-1}.s^{-1}$ (see Appendix A for details). As shown in Fig. 6, a relatively good match was obtained between the experimental and simulated CVs at two different scan rates (*v* = 100 $V.s^{-1}$ and *v* = 1 $V.s^{-1}$) indicating that the value of k_{dim} found by using equation (1) was reasonable.

3.2 Computational studies

The electrochemical study provided strong evidence that the mechanism of oxidative dimerization of **1a-f** derivatives depends on the nature of the R group, i.e. radical-radical (RRD) coupling for R = NMe_2 and OMe, and radical-substrate (RSD) coupling for R = H, Br, CO_2Me and NO_2 (Table 1). To rationalize this experimental result, the electronic structures of $[^{R}PhMP]^{0/+}$ and $[Bis^{R}PhMP]^{+/2+}$ have been calculated for R = NMe_2, H and NO_2. The range of

quantum chemical methods applicable to study the dimerization of ^{R}PhMP derivatives is restricted by the large size of the dimer (ca. 100 atoms). Here, all electronic structure calculations were carried out using the HF-3c method, which is a fast Hartee-Fock method developed for accurate computation of large organic molecules [32].

The calculated structure of **1b** (R = NMe_2) is shown in Fig. S1. Selected values of bond length and angle from the X-ray and calculated structures are displayed in Table S1. The average absolute error on the calculated bond lengths is better than 0.02 Å, indicating that the chosen theoretical method appropriately describes the electronic structure of this family of compounds. Similarly, a good agreement was found between the X-ray structure of [Bis-FcMP]$^{2+}$ [28, 30] and the calculated structure of **2b**$^{2+}$ (Fig. S2). The length of the C–C bond formed in the dimerization process is 1.53 Å and 1.56 Å in [Bis-FcMP]$^{2+}$ and **2b**$^{2+}$, respectively. Moreover, the dihedral angle between the two Fc groups trans to the C–C bond of the dimer is 180º and that between the two ^{NMe2}Ph groups is 175º. These results further show that electronic structure calculations are consistent with a σ-dimer, in which the ^{R}Ph moieties have little steric effects.

Table 2. Spin population in the gas phase and solvent (i.e. CH_2Cl_2) on the carbon C_{30} involved in the dimerization of **1a**$^{+\bullet}$, **1b**$^{+\bullet}$ and **1f**$^{+\bullet}$ (see atom numbers on Fig. S1).

	R	**Gas**	**Solvent**
1b$^{+\bullet}$	NMe_2	0.716	0.880
1a$^{+\bullet}$	H	0.914	0.938
1f$^{+\bullet}$	NO_2	0.932	0.953

Since dimerization occurs upon oxidation of compound **1**, we first analyzed the spin population on the carbon involved in the formation of the σ-dimer for three selected radical cations $\mathbf{1}^{+\bullet}$. As shown in Table 2, the spin population on C_{30} (see atom numbers on Fig. S1) increases with the electrophilic character of the R group in both gas phase and solvent. Noticeably, the spin density on this carbon atom is significantly larger for $\mathbf{1a}^{+\bullet}$ (R = H) or $\mathbf{1f}^{+\bullet}$ (NO_2) than for $\mathbf{1b}^{+\bullet}$ (R = NMe_2), reaching a value of almost +1 for $\mathbf{1f}^{+\bullet}$ in CH_2Cl_2 (Table 2). Such a result suggests that the radical-radical dimerization is less favored in the case of $\mathbf{1a}^{+\bullet}$ and $\mathbf{1f}^{+\bullet}$, probably because of strong electrostatic repulsion, even in presence of solvent.

As shown in Scheme 2, the coupling of two $\mathbf{1}^{+\bullet}$ radicals produces a doubly-charged dimer $\mathbf{2}^{2+}$, while the radical-substrate dimerization yields a singly-charged dimer $\mathbf{2}^{+}$ which can be further oxidized. The relative stability of these two different dimers ($\mathbf{2}^{+}$ and $\mathbf{2}^{2+}$) can be estimated from the values of the C_1-C_{33} bond length (see atom numbers on Fig. S2), as well from its Mayer bond order [38]. Fig. 7 and 8 display the results obtained for the three series of dimers according to the Brown constant of the R group (R=H, NMe_2 and NO_2). The C_1-C_{33} bond length is smaller for $\mathbf{2b}^{2+}$ (Fig. 7, black square) than for $\mathbf{2b}^{+}$ (Fig. 7, red disk), whereas the opposite result is obtained for $\mathbf{(2a)}^{2+/+}$ and $\mathbf{(2f)}^{2+/+}$ dimers. In addition, the Mayer bond order is higher for $\mathbf{2b}^{2+}$ than for $\mathbf{2b}^{+}$, conversely to the two others series (Fig. 8). These results strongly suggest that the doubly-charged dimer $\mathbf{2b}^{2+}$ is relatively more stable than the mono-charged one $\mathbf{2b}^{+}$, consistent with a RRD process. In contrast, the shorter C_1-C_{33} bond and the larger Mayer order in the monocationic dimer than in the dicationic one for R=H and R=NO_2 indicates that the RSD process is likely favored in those cases, in agreement with experimental data.

Fig. 7

Fig. 7. Plots of calculated C-C bond length *vs*. Brown contant (σ^+) of the R group for doubly-charged $\mathbf{2}^{2+}$ (black squares) and mono-charged $\mathbf{2}^{+}$ dimers (R = NMe_2, H, NO_2).

Fig. 8.

Fig. 8. Plots of Mayer C-C bond order *vs*. Brown contant (σ^+) of the R group for doubly-charged $\mathbf{2}^{2+}$ (black squares) and mono-charged $\mathbf{2}^{+}$ dimers (R = NMe_2, H, NO_2).

Table 3. Free energy change (kcal.mol^{-1}) in the gas phase and in solvent (i.e. CH_2Cl_2) for homolytic and heterolytic C–C bond cleavage in $\mathbf{2}^{2+}$ and $\mathbf{2}^{+}$ dimers.

	$\mathbf{2}^{2+} \rightarrow \mathbf{1}^{+} + \mathbf{1}^{+}$ **(homolytic)**		$\mathbf{2}^{+} \rightarrow \mathbf{1}^{+} + \mathbf{1}$ **(heterolytic)**	
R	**Gas**	**Solvent**	**Gas**	**Solvent**
NMe_2	–63.2	–36.8	39.9	37.6
H	–45.6	–18.0	49.8	48.8
NO_2	–120.3	–125.9	93.6	91.3

The free energy changes associated with C–C bond cleavage for $\mathbf{2}^{2+}$ and $\mathbf{2}^{+}$ dimers are listed in Table 3. Homolytic cleavage produces two cationic monomers from a doubly charged dimer, i.e. $\mathbf{2}^{2+} \rightarrow \mathbf{1}^{+} + \mathbf{1}^{+}$, while heterolytic cleavage produces one cationic and one neutral monomer from a singly charged dimer, i.e. $\mathbf{2}^{+} \rightarrow \mathbf{1}^{+} + \mathbf{1}$. Homolytic bond cleavages are all exergonic whereas heterolytic cleavages are all endergonic, indicating that a symmetric bond dissociation is always thermodynamically favored. On the other hand, the free energy change associated with the heterolytic bond cleavage increases in the order $NMe_2 < H < NO_2$, in both

the gas phase and solvent. Although this result does not provide any information on the kinetics of dimerization, it suggests that RS-coupling is less thermodynamically disfavored for R = NO_2 than for R = NMe_2.

4. Conclusions

The voltammetric studies of the R-substituted phenylmethylenepyrans **1a-f** have shown that the irreversible oxidation potential leads to the formation of bis-pyrylium σ-dimers **(2a-f)**$^{2+}$. Although the oxidation potential is fully dependent on the electrophilic property of the substituent, the potential of reduction of **(2a-f)**$^{2+}$ cleaving the C-C bond and yielding back **1a-f**, does not vary significantly with R. Our voltammetric analyses also demonstrate that the intermolecular dimerization follows either a radical-radical or radical-substrate pathway according to the nature of the substituting moiety. Hence, dimerization occurs merely through a radical-radical process with electrodonating groups such as NMe_2 and OMe, whereas RSD is observed for the other phenylmethylenepyrans. Electronic structure calculations suggest that this trend results from the inversion of the relative stabilities of the mono- and doubly-charged dimers with R. The kinetics of the RRD reaction have also been investigated by low-temperature electrochemical voltammetry (175 K), and room-temperature high scan rate CV. The electrochemical analysis, supported by voltammetric simulations, suggest a rather fast process with $k_{dim} = 10^7$ $M^{-1}.s^{-1}$. From these results, future works will aim at developing new PhMPs compounds in order to slow down the dimerization coupling, by incorporation of bulky groups on the pyran moiety. Under such conditions, experimental and theoretical approaches will be carried out to further elucidate the mechanistic pathways. These results will be of interest for optimizing further development of redox chromophores with fast switching time, on the basis of our previous studies [26].

Acknowledgments

Financial support by Agence Nationale pour la Recherche (ANR-13-BSO7-0018), Conseil Général du Finistère, and Université de Bretagne Occidentale. I.L. acknowledges support from the European Commission under the Campus Prestige progamme (PRESTIGE-2015-2-0019).

Appendix A. Supplementary data

Supplementary data to this article can be found online.

References

[1] C. Amatore, J. Pinson, J.M. Savéant, Are anion radicals unable to undergo radical-radical dimerization?, J. Electroanal. Chem. Int. Electrochem., 137 (1982) 143-148.

[2] C. Amatore, D. Garreau, M. Hammi, J. Pinson, J.M. Savéant, Kinetic analysis of reversible electrodimerization reactions by the combined use of double potential step chronoamperometry and linear sweep voltammetry, J. Electroanal. Chem. Int. Electrochem., 184 (1985) 1-24.

[3] V. Mazine, J. Heinze, Dimerization of electrochemically generated radical ions under high pressure, J. Phys. Chem. A, 108 (2004) 230-235.

[4] N.A. Macías-Ruvalcaba, J.P. Telo, D.H. Evans, Studies of the electrochemical reduction of some dinitroaromatics, J. Electroanal. Chem., 600 (2007) 294-302.

[5] N.A. Macías-Ruvalcaba, G.A.N. Felton, D.H. Evans, Contrasting behavior in the reduction of 1,2-acenaphthylenedione and 1,2-aceanthrylenedione. Two types of reversible dimerization of anion radicals, J. Phys. Chem. C, 113 (2009) 338-345.

[6] P.D. Astudillo Sánchez, D.H. Evans, Reversible dimerization of the anion radicals of some dicyanonaphthalenes, J. Electroanal. Chem., 660 (2011) 91-96.

[7] Y.S. Tan, Y. Yue, R.D. Webster, Competing hydrogen-bonding, decomposition, and reversible dimerization mechanisms during the one- and two-electron electrochemical reduction of retinal (vitamin A), J. Phys. Chem. B, 117 (2013) 9371-9379.

[8] V.D. Parker, Radical Reactivity of Radical Ions in Solution. Radical--Radical and Radical--Substrate Coupling Mechanisms, Acta Chemica Scandinavica, 52 (1998) 154-159.

[9] R. Rathore, P. Le Magueres, S.V. Lindeman, J.K. Kochi, A redox-controlled molecular switch based on the rversible C−C bond formation in octamethoxytetraphenylene, Angew. Chem. Int. Ed. Engl., 39 (2000) 809-812.

[10] H. El-Desoky, J. Heinze, M.M. Ghoneim, Electrodimerization of cyano-substituted derivatives of anthracene and naphthalene, Electrochem. Commun., 3 (2001) 697-702.

[11] J. Heinze, C. Willmann, P. Bäuerle, Evidence for σ dimerization during anodic redox switching of 1,3,5-tripyrrolidinobenzene: A new molecular switch, Angew. Chem. Int. Ed. Engl., 40 (2001) 2861-2864.

[12] C. Kahlfuss, E. Saint-Aman, C. Bucher, Redox-controlled intramolecular motions triggered by π-dimerization and pimerization processes, Wiley2015.

[13] C. Kahlfuss, E. Metay, M.C. Duclos, M. Lemaire, A. Milet, E. Saint-Aman, C. Bucher, Chemically and electrochemically triggered assembly of viologen radicals: towards multiaddressable molecular switches, Chem. Eur. J., 21 (2015) 2090-2106.

[14] I. Gallardo, G. Guirado, J. Marquet, N. Vila, Evidence for a pi dimer in the electrochemical reduction of 1,3,5-trinitrobenzene: a reversible N2-fixation system, Angew. Chem. Int. Ed. Engl., 46 (2007) 1321-1325.

[15] N. Le Poul, B. Colasson, Electrochemically and chemically induced redox processes in molecular machines, ChemElectroChem, 2 (2015) 475-496.

[16] S. Hünig, C.A. Briehn, P. Bäuerle, A. Emge, Electrochromics by intramolecular redox switching of single bonds, Chem. Eur. J., 7 (2001) 2745-2757.

[17] T. Suzuki, H. Higuchi, M. Ohkita, T. Tsuji, Dual-mode electrochromism switched by proton transfer: dynamic redox properties of bis(diarylmethylenium)-type dyes, Chem. Commun., (2001) 1574-1575.

[18] A.B. Nepomnyashchii, M. Broring, J. Ahrens, A.J. Bard, Chemical and electrochemical dimerization of BODIPY compounds: electrogenerated chemiluminescent detection of dimer formation, J. Am. Chem. Soc., 133 (2011) 19498-19504.

[19] L. Kortekaas, O. Ivashenko, J.T. van Herpt, W.R. Browne, A remarkable multitasking double spiropyran: bidirectional visible-light switching of polymer-coated surfaces with dual redox and proton gating, J. Am. Chem. Soc., 138 (2016) 1301-1312.

[20] J.R. Brandt, L. Pospisil, L. Bednarova, R.C. da Costa, A.J.P. White, T. Mori, F. Teply, M.J. Fuchter, Intense redox-driven chiroptical switching with a 580 mV hysteresis actuated through reversible dimerization of an azoniahelicene, Chem. Commun., 53 (2017) 9059-9062.

[21] S. Gauthier, B. Caro, F. Robin-Le Guen, N. Bhuvanesh, J.A. Gladysz, L. Wojcik, N. Le Poul, A. Planchat, Y. Pellegrin, E. Blart, D. Jacquemin, F. Odobel, Synthesis, photovoltaic performances and TD-DFT modeling of push-pull diacetylide platinum complexes in TiO2 based dye-sensitized solar cells, Dalton Trans., 43 (2014) 11233-11242.

[22] S. Gauthier, A. Porter, S. Achelle, T. Roisnel, V. Dorcet, A. Barsella, N. Le Poul, P. Guevara Level, D. Jacquemin, F. Robin-Le Guen, Mono- and diplatinum polyynediyl complexes as potential push–pull chromophores: synthesis, characterization, TD-DFT modeling, and photophysical and NLO Properties, Organometallics, 37 (2018) 2232-2244.

[23] R.J. Durand, S. Gauthier, S. Achelle, T. Groizard, S. Kahlal, J.Y. Saillard, A. Barsella, N. Le Poul, F.R. Le Guen, Push-pull D-pi-Ru-pi-A chromophores: synthesis and electrochemical, photophysical and second-order nonlinear optical properties, Dalton Trans., 47 (2018) 3965-3975.

[24] R.J. Durand, S. Gauthier, S. Achelle, S. Kahlal, J.-Y. Saillard, A. Barsella, L. Wojcik, N. Le Poul, F. Robin-Le Guen, Incorporation of a platinum center in the pi-conjugated core of push-pull chromophores for nonlinear optics (NLO), Dalton Trans., 46 (2017) 3059-3069.

[25] P. Hapiot, D. Lorcy, A. Tallec, R. Carlier, A. Robert, Mechanism of dimerization of 1,4-dithiafulvenes into TTF Vinylogues, J. Phys. Chem., 100 (1996) 14823-14827.

[26] L. Wojcik, F. Michaud, S. Gauthier, N. Cabon, P. Le Poul, F. Gloaguen, N. Le Poul, Reversible redox switching of chromophoric phenylmethylenepyrans by carbon-carbon bond making/breaking, J. Org. Chem., 82 (2017) 12395-12405.

[27] P. Le Poul, N. Le Poul, S. Golhen, F. Robin-Le Guen, B. Caro, The synthesis of flexible tetrapyridylethanes from pyridylpyrylium dications, New J. Chem., 40 (2016) 5666-5669.

[28] F. Ba, N. Cabon, P. Le Poul, S. Kahlal, J.-Y. Saillard, N. Le Poul, S. Golhen, B. Caro, F. Robin-Le Guen, Diferrocenylpyrylium salts and electron rich bispyran from oxidative coupling of ferrocenylpyran. Example of redox systems switched by proton transfer, New J. Chem., 37 (2013) 2066-2081.

[29] F. Ba, F. Robin-Le Guen, N. Cabon, P. Le Poul, S. Golhen, N. Le Poul, B. Caro, Ferrocenyl and pyridyl methylenepyrans as potential precursors of organometallic electron-rich extended bipyrans: Synthesis, characterization and crystal structure, J. Organomet. Chem., 695 (2010) 235-243.

[30] F. Ba, N. Cabon, F. Robin-Le Guen, P. Le Poul, N. Le Poul, Y. Le Mest, S. Golhen, B. Caro, Diferrocenylbispyrylium salts and electron-rich diferrocenylbispyran from oxidative coupling of ferrocenylpyran. induced electron transfer C−C bond making/breaking involving a metallocenyl radical intermediate, Organometallics, 27 (2008) 6396-6399.

[31] I. Lopez, R. Cao, D.A. Quist, K.D. Karlin, N. Le Poul, Direct determination of electron-transfer properties of dicopper-bound reduced dioxygen species by a cryo-spectroelectrochemical approach, Chem. Eur. J., 23 (2017) 18314-18319.

[32] R. Sure, S. Grimme, Corrected small basis set Hartree-Fock method for large systems, J. Comput. Chem., 34 (2013) 1672-1685.

[33] F. Neese, The ORCA program system, Wiley Interdisciplinary Reviews: Computational Molecular Science, 2 (2012) 73-78.

[34] M.D. Hanwell, D.E. Curtis, D.C. Lonie, T. Vandermeersch, E. Zurek, G.R. Hutchison, Avogadro: an advanced semantic chemical editor, visualization, and analysis platform, J Cheminform, 4 (2012) 17.

[35] S. Sinnecker, A. Rajendran, A. Klamt, M. Diedenhofen, F. Neese, Calculation of solvent shifts on electronic g-tensors with the conductor-like screening model (COSMO) and its self-consistent generalization to real solvents (direct COSMO-RS), J. Phys. Chem. A, 110 (2006) 2235-2245.

[36] G. De Leener, D. Over, C. Smet, D. Cornut, A.G. Porras-Gutierrez, I. Lopez, B. Douziech, N. Le Poul, F. Topic, K. Rissanen, Y. Le Mest, I. Jabin, O. Reinaud, "Two-Story" calix[6]arene-based zinc and copper complexes: structure, properties, and O2 binding, Inorg. Chem., 56 (2017) 10971-10983.

[37] J.-M. Savéant, Elements of molecular and biomolecular electrochemistry: an electrochemical approach to electron transfer chemistry, Wiley2006.

[38] I. Mayer, Charge, bond order and valence in the AB initio SCF theory, Chem. Phys. Lett., 97 (1983) 270-274.

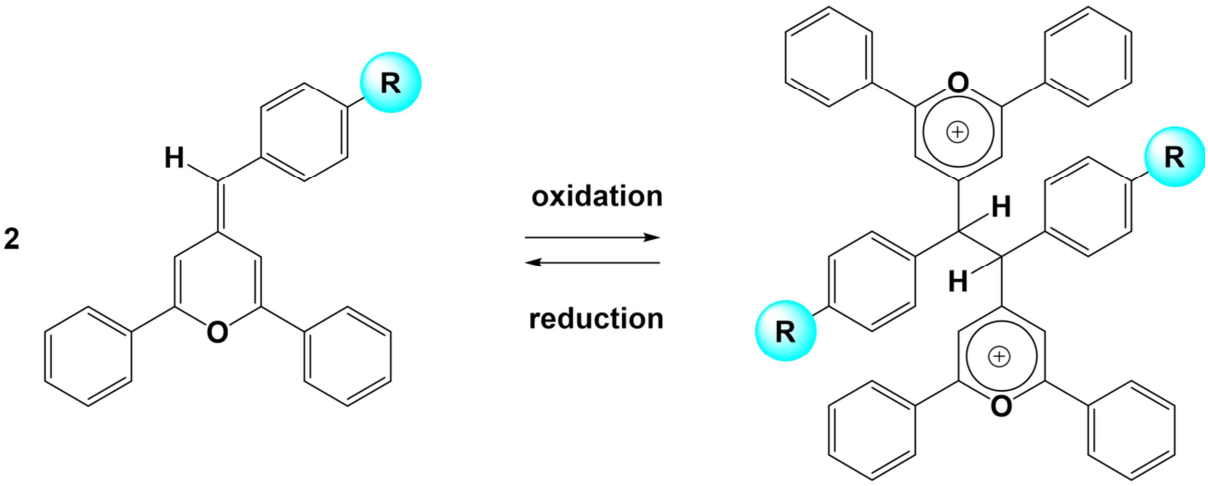

1a (R = H)

1b (R = NMe_2)

1c (R = OMe)

1d (R = CO_2Me)

1e (R = Br)

1f (R = NO_2)

$2a^{2+}$ (R = H)

$2b^{2+}$ (R = NMe_2)

$2c^{2+}$ (R = OMe)

$2d^{2+}$ (R = CO_2Me)

$2e^{2+}$ (R = Br)

$2f^{2+}$ (R = NO_2)

Scheme 1. C-C bond making/breaking by oxidation of R-substituted phenylmethylenepyrans **1a-f** and reduction of their bis-pyrylium derivatives **(2a-f)**$^{2+}$.

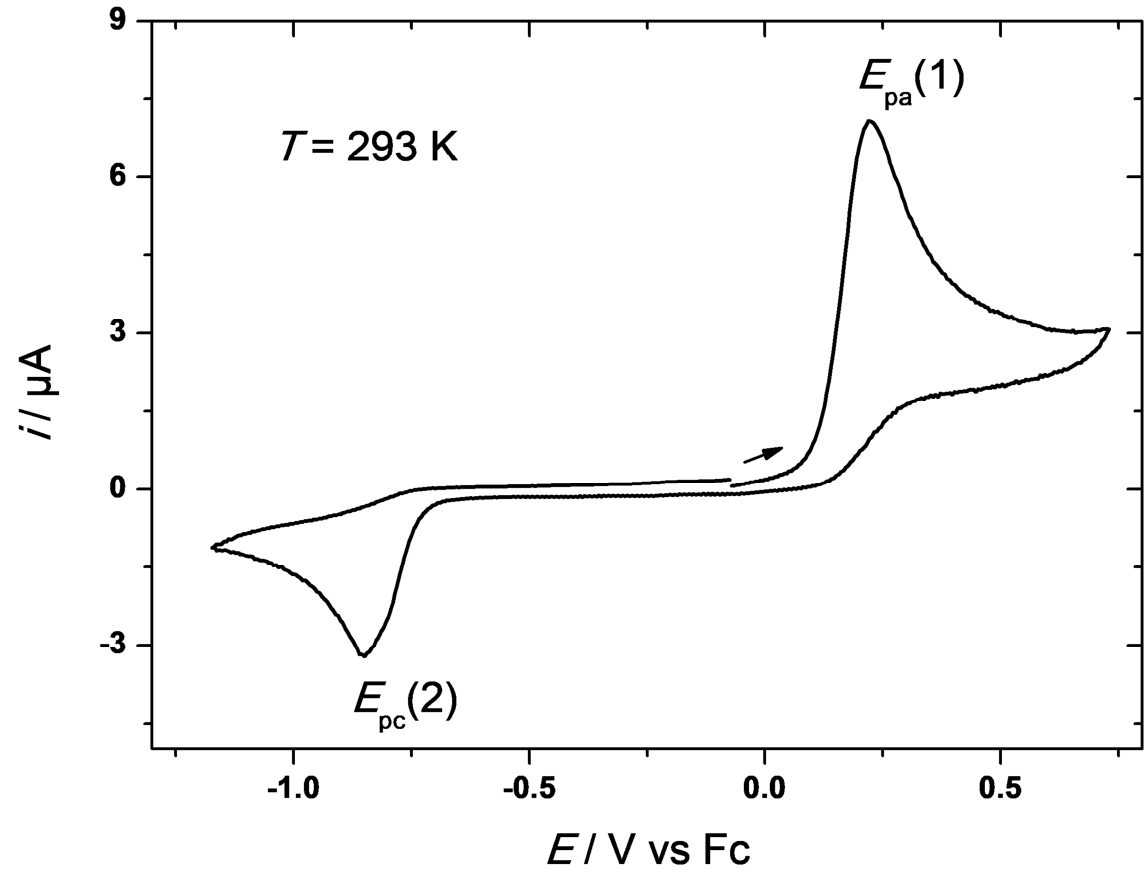

Fig. 1. CV (v = 0.1 V.s^{-1}) at a Pt electrode (diam. 3mm) of compound **1a** (C = 1mM) in CH_2Cl_2/NBu_4PF_6 0.1 M under argon at T = 293 K.

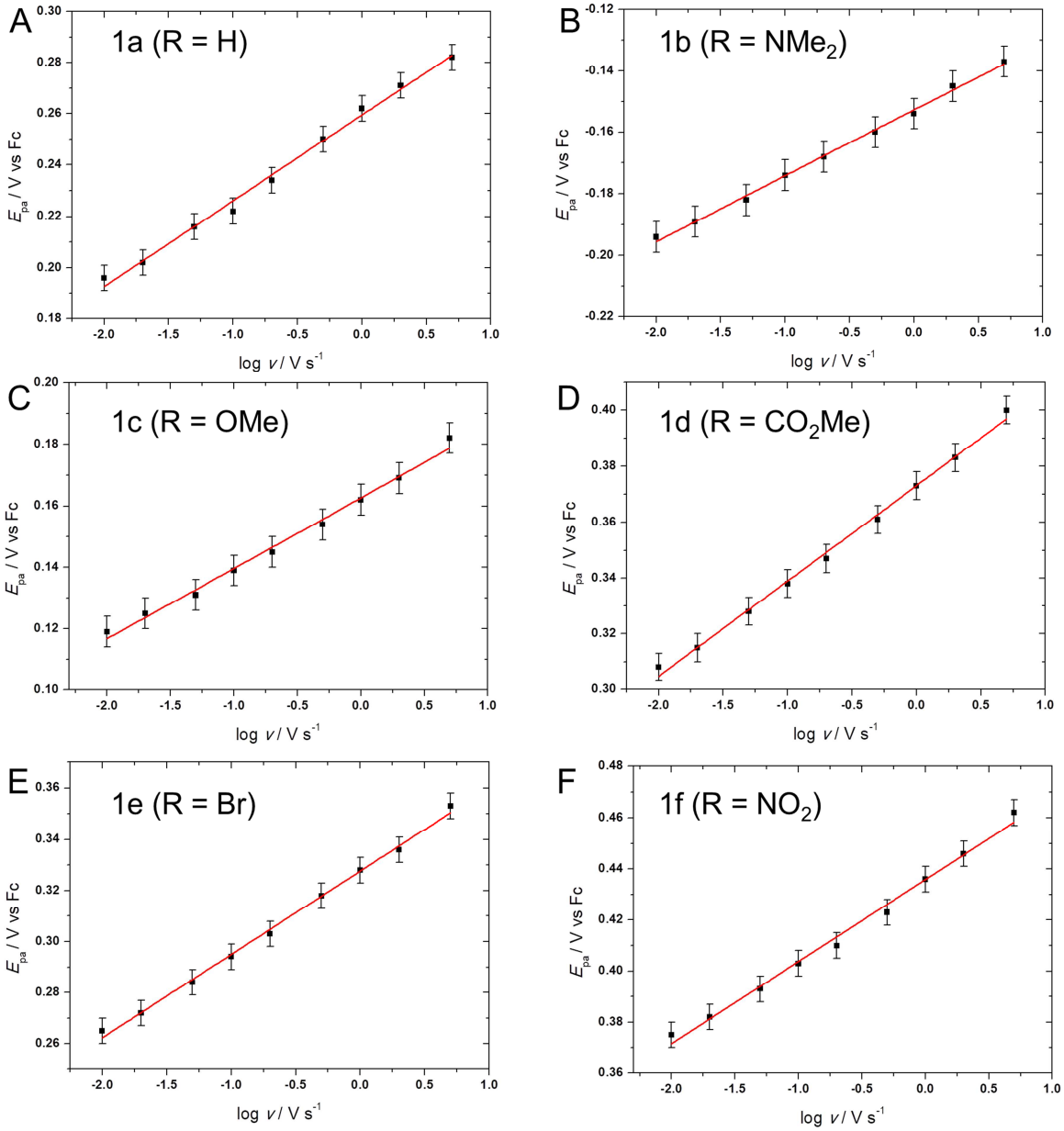

Fig. 2. Plots of E_{pa} *vs*. log *v* for compounds A) **1a** (R=H); B) **1b** (R=NMe_2); C) **1c** (R=OMe); D) **1d** (R=CO_2Me); E) **1e** (R=Br); F) **1f** (R = NO_2); (*C* = 0.5 mM).

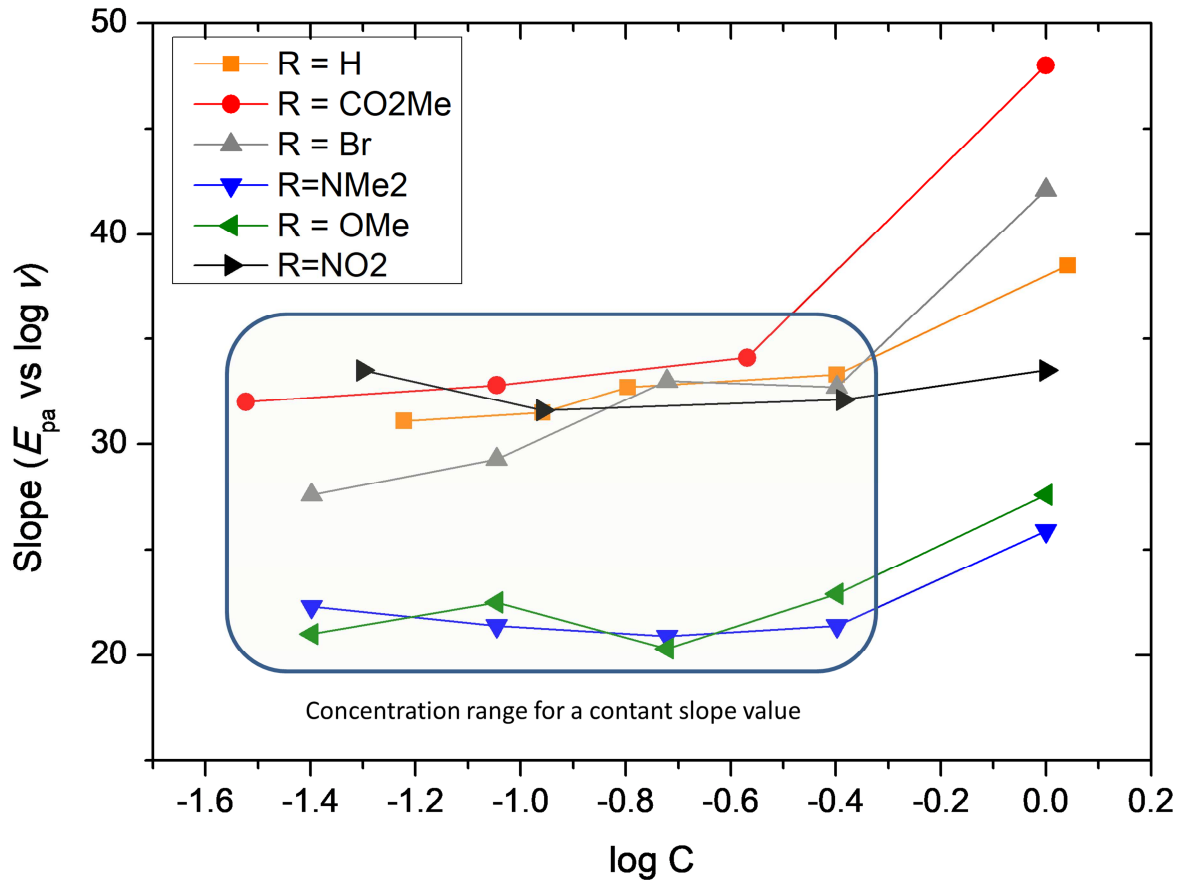

Fig. 3. Plots of slope of (E_{pa} *vs*. log *v*) against log *C* for **1a-f**.

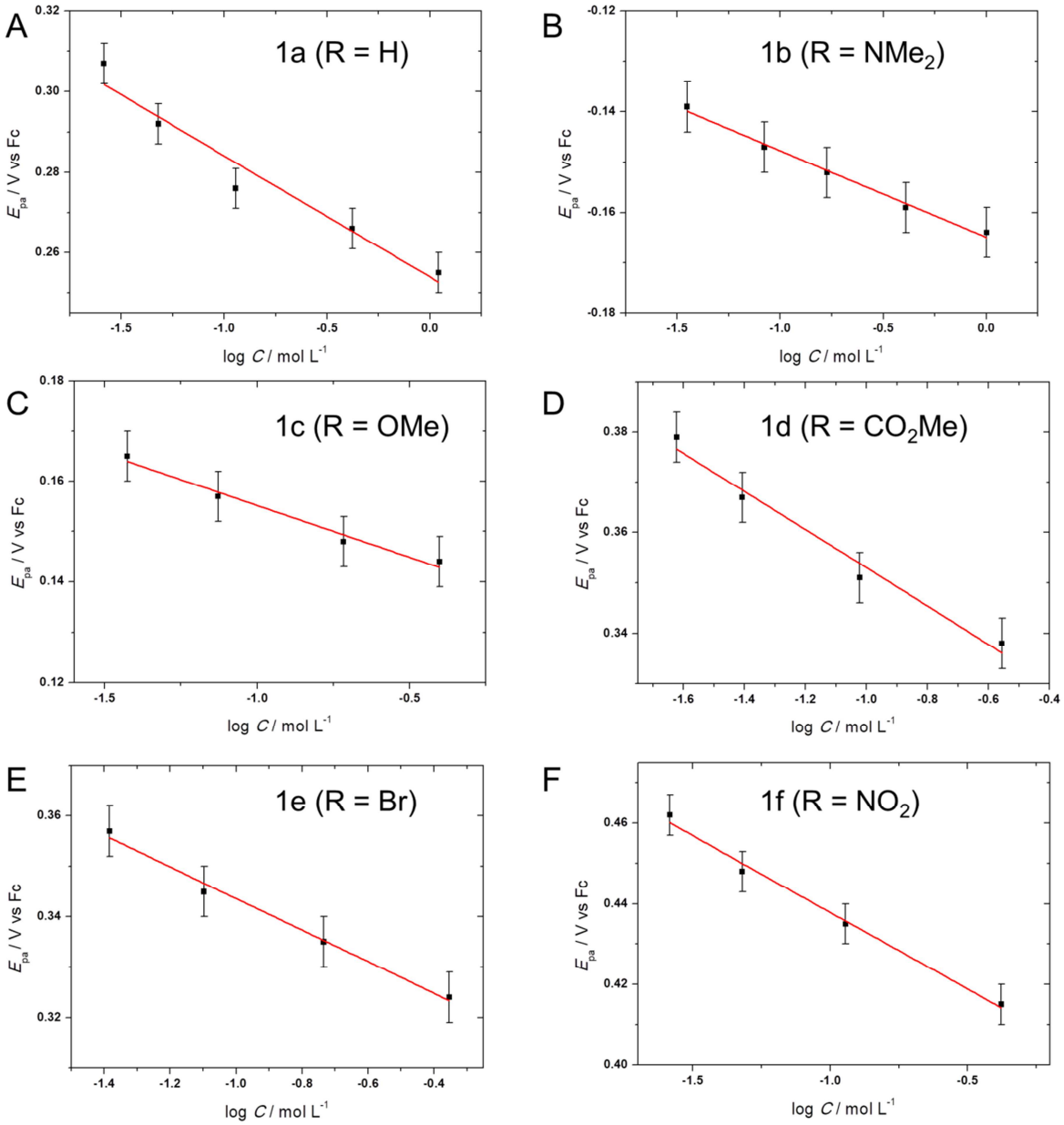

Fig. 4. Plots of E_{pa} vs log C for compounds A) **1a** (R=H); B) **1b** (R=NMe_2); C) **1c** (R=OMe); D) **1d** (R=CO_2Me); E) **1e** (R=Br); F) **1f** (R = NO_2); (v = 0.1 $V.s^{-1}$).

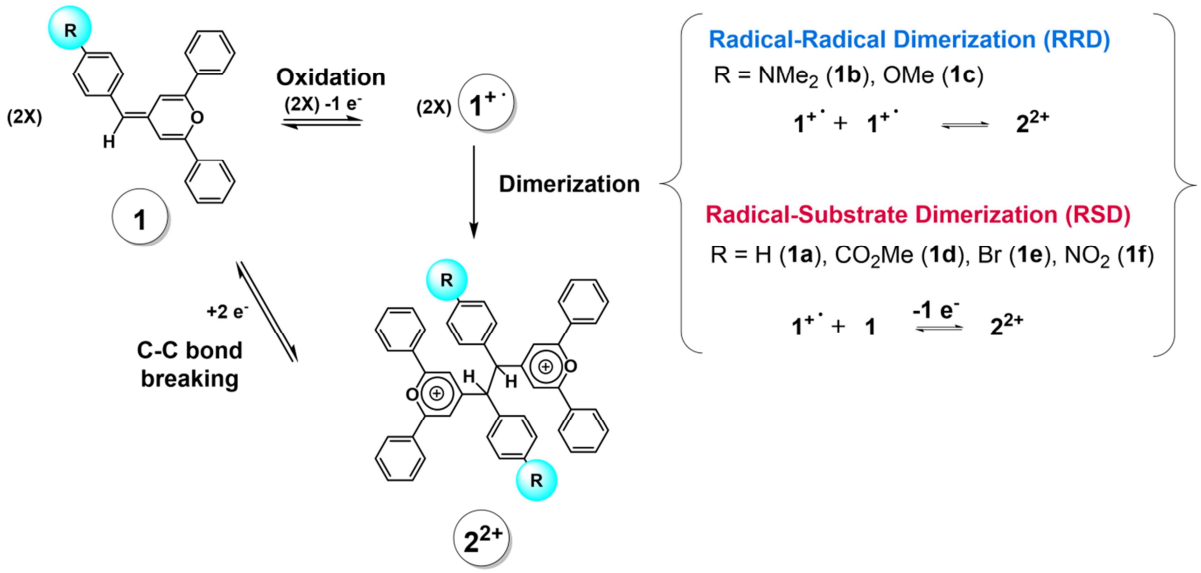

Scheme 2. Schematic pathway for the C-C bond making/breaking of R-substituted phenylmethylenepyran **1a-f** compounds upon electron transfer.

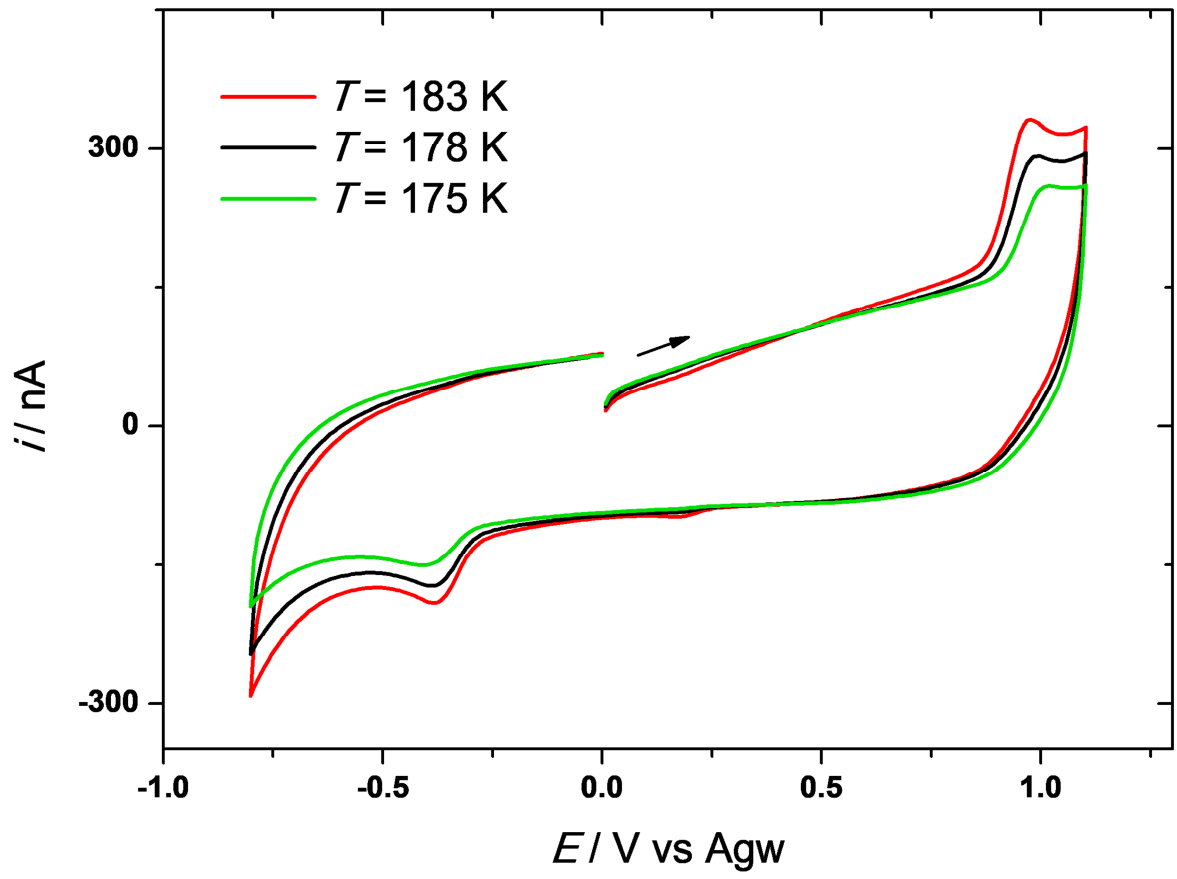

Fig. 5. CVs (v = 0.1 V.s^{-1}) at a Pt electrode (diam. 1mm) of compound **1d** (0.04 mM) in CH_2Cl_2/NBu_4PF_6 0.1 M under argon for 175 K < T < 183 K.

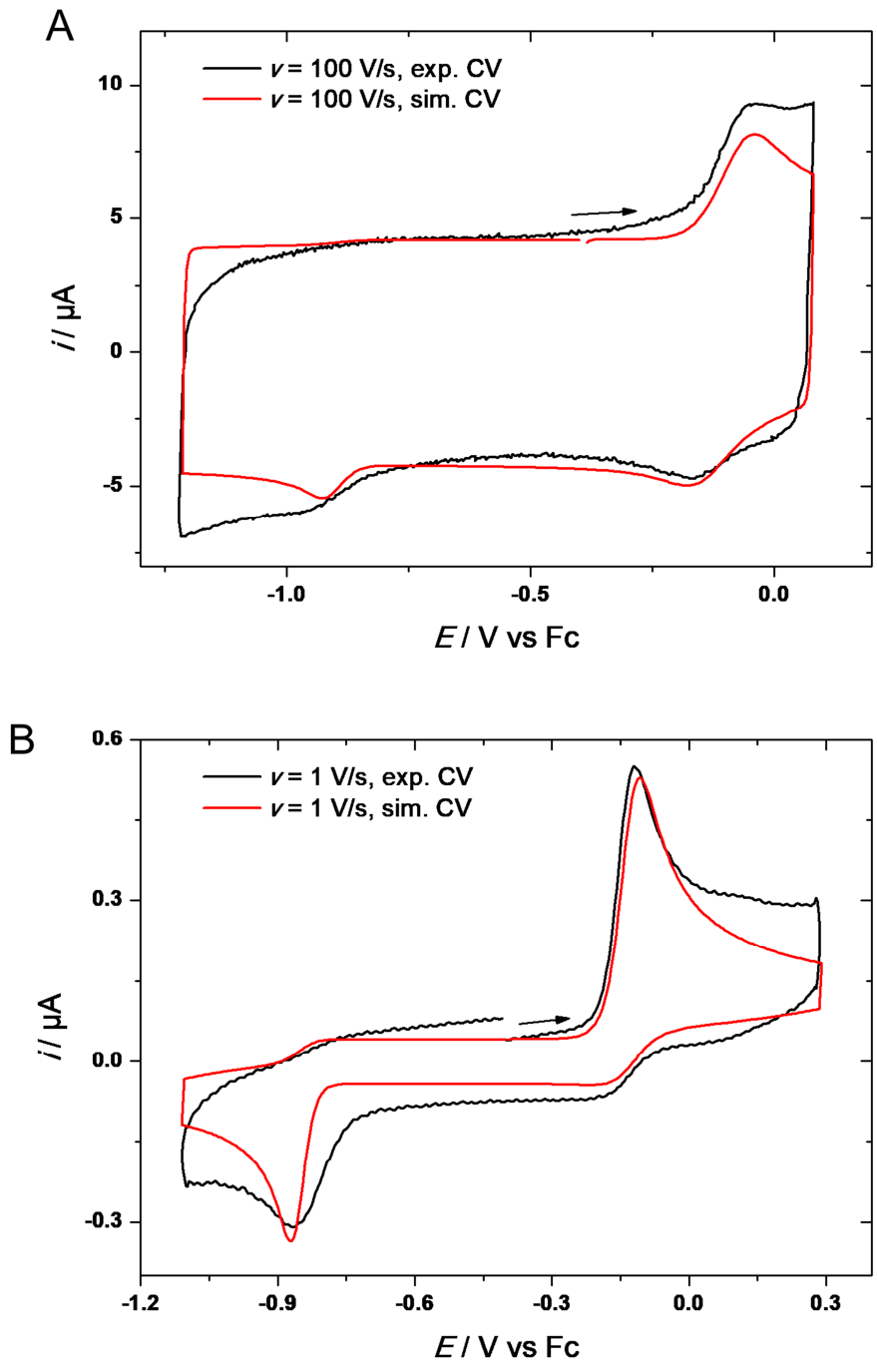

Fig. 6. Experimental (black) and simulated (red) CVs at A) ν = 100 V.s^{-1} and B) ν = 1 V.s^{-1} of compound **1b** (C = 0.09 mM) at a Pt electrode (diam. 1mm) in CH_2Cl_2/NBu_4PF_6 0.1 M. (for details, see Appendix A).

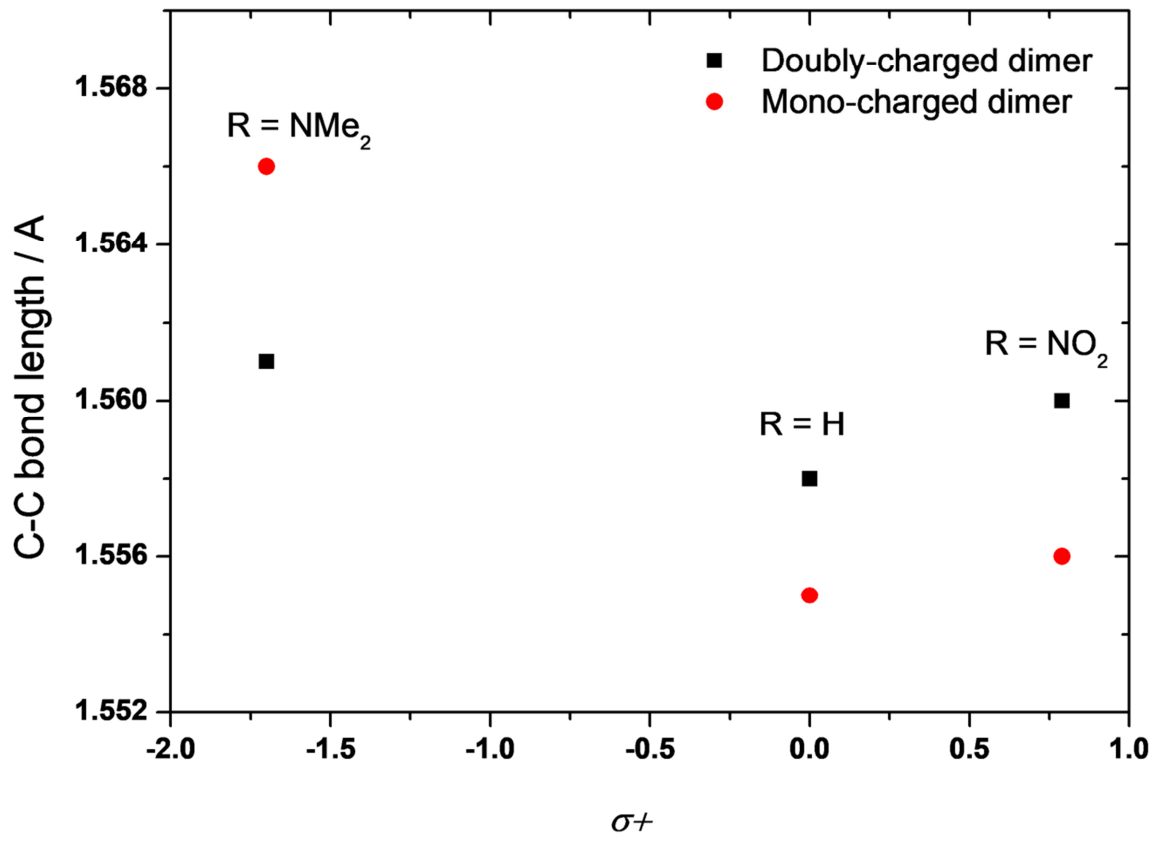

Fig. 7. Plots of calculated C-C bond length *vs*. Brown contant (σ^+) of the R group for doubly-charged $\mathbf{2}^{2+}$ (black squares) and mono-charged $\mathbf{2}^{+}$ dimers (R = NMe_2, H, NO_2).

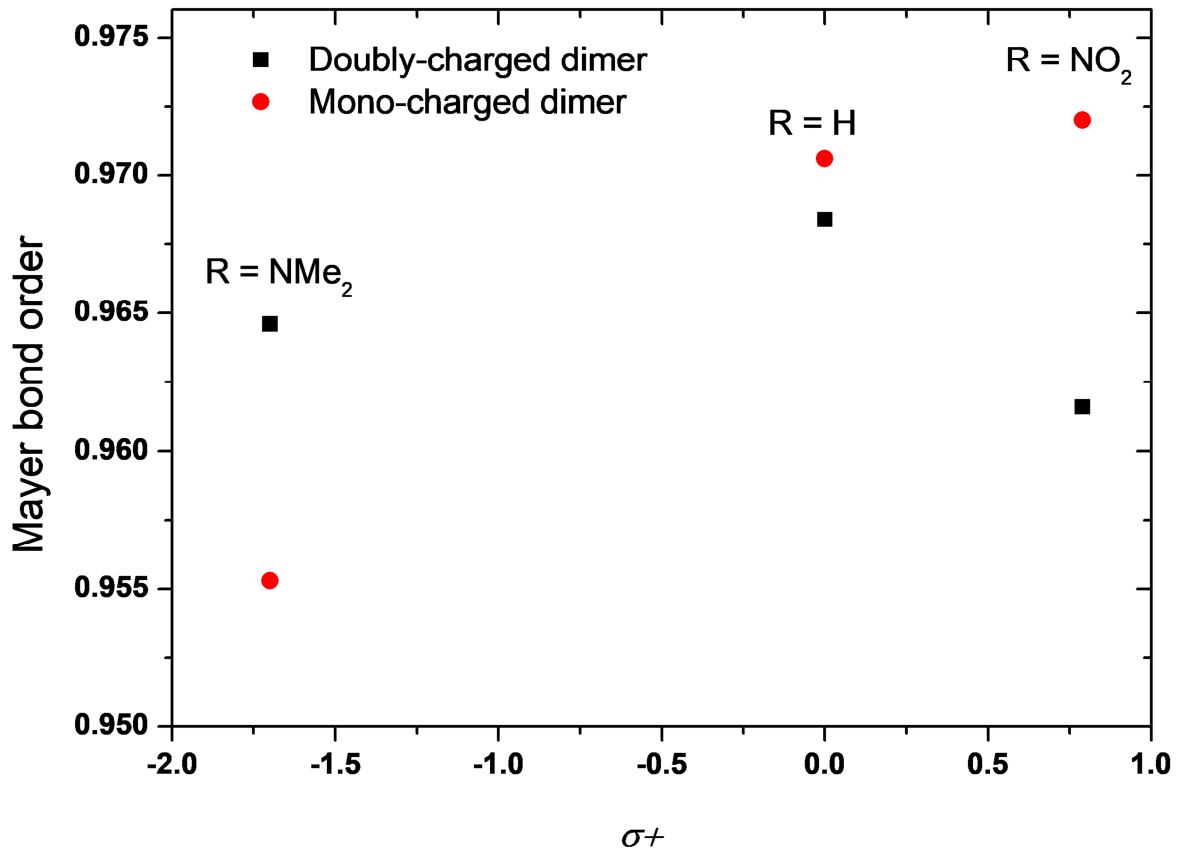

Fig. 8. Plots of Mayer C-C bond order *vs*. Brown contant (σ^+) of the R group for doubly-charged $\mathbf{2}^{2+}$ (black squares) and mono-charged $\mathbf{2}^{+}$ dimers (R = NMe_2, H, NO_2).